Solid-State Electronics Vol. 33, No. 7, pp. 923–933, 1990
Printed in Great Britain

0038-1101/90 $3.00 + 0.00
Pergamon Press plc

A PHYSICS BASED ANALYTICAL MOSFET MODEL WITH ACCURATE FIELD DEPENDENT MOBILITY

PREDRAG HABAŠ*
Institute for Microelectronics, Technical University Vienna, Gußhausstrasse 27-29, 1040 Vienna, Austria

(*Received* 19 *September* 1989; *in revised form* 19 *December* 1989)

Abstract—A new approach to the modeling of short-channel MOSFETs in the triode region is proposed. A system of equations for an accurate quasi-1-D-formulation of the current transport in MOSFETs is presented. A highly accurate description of the local normal effective field-dependent surface mobility is included. The mobility degradation due to the parallel field is modeled by a hyperbolic formula for *P*-channel and by Jaggi's expression for *N*-channel MOSFETs. The mobility models are examined by comparing with several experimental data. The system includes a precise modeling of the inversion layer charge and surface potential, and it is valid in both weak and strong inversion. Using novel approaches an approximate solution in the triode region is derived analytically. The obtained expressions for the current are explicit. An error analysis of the analytical current models is carried out by comparing with a numerical solution of the starting quasi-1-D-formulation. As a result of the error analysis the simplest final expression for the drain current is proposed. Some further extensions of the model are noted.

1. INTRODUCTION

Due to non-uniform scaling of the supply voltages and dimensions, high normal and parallel fields occur in modern MOSFETs. These fields affect significantly the carrier mobilities. Due to 2-D and 3-D effects and field dependent mobilities it is more complicated to model analytically the short-channel MOSFETs. In addition it is necessary to model precisely the channel charge (due to thin oxides), to take into account the real doping profile and the source and the drain series resistances. In this paper we will not give a model for all operating regions, which includes all previous effects. It is not possible to derive exactly such an analytical model. On the other hand, there are several approximate models with empirical fitting parameters in the literature[1,2]. We restrict ourselves to the local normal and parallel field-dependent mobility and to the precise modeling of the inversion layer charge. In this paper these effects are included precisely in the drain current model using novel analytical approaches. For the sake of simplicity, a homogeneously doped substrate is assumed in the present model.

In Section 2 the modeling of the inversion layer charge and the surface potential is discussed in detail. The mobility models for simultaneous normal and parallel fields are examined. The drain current model in the triode region is derived in Section 3, where an error analysis and discussion about the qualitative behaviour of the model are carried out. Further extensions of the presented model are considered briefly in Section 4.

*On leave from the Institute for Power and Electronics, Faculty of Technical Sciences, University of Novi Sad, Yugoslavia.

2. MODELING OF THE RELEVANT PHYSICAL QUANTITIES

In this section the analysis of the charge and the mobility in the inversion layer is given. These quantities directly contribute to the drain current. We assume a homogeneously doped substrate with a donor concentration N_B. In the triode region gradual channel approximation (G.C.A.) and "capacitive formula" are valid

$$\left|\frac{\partial E_x}{\partial x}\right| \gg \left|\frac{\partial E_y}{\partial y}\right| \quad (1a)$$

$$|E_x| \gg |E_y| \quad (1b)$$

where x, y are the coordinates normal and parallel to the Si–SiO_2 interface and E_x, E_y are the normal and parallel electric field in the channel. We assume Maxwell–Boltzmann (MB) statistics for electrons in the inversion layer for the moment. Using eqns (1a,b) and integrating Poisson's equation (from surface toward the bulk) we obtain in weak and strong inversion after comparison with Gauss's law:

$$U_{GS} - V_{FB} - V - \varphi_S = D\left[V + \varphi_S - U_{BS} - U_T + U_T \exp\left(\frac{\varphi_S - 2\varphi_B}{U_T}\right)\right]^{1/2} \quad (2)$$

Here are: V_{FB} flat-band voltage; V potential difference between quasi-Fermi level for electrons in the inversion layer and Fermi level in the source; φ_B

Fermi-barrier in the bulk; φ_S relative surface potential;† $D = \sqrt{2e\epsilon_s N_B}/C_o$, $C_o = \epsilon_{ox}/t_{ox}$, t_{ox} oxide thickness; U_T thermal voltage and U_{GS}, U_{BS} supply voltages. φ_S can be calculated for a given V, U_{GS} and U_{BS} from the implicit eqn (2) using some efficient numerical approach. The expression (2) is consistent with the well known definitions of the operating regions and the theoretical threshold: $\varphi_B \leqslant \varphi_S < 2\varphi_B$ weak inversion,

$$\varphi_S = 2\varphi_B \Leftrightarrow U_{GS} = U_t = V_{FB} + 2\varphi_B + D\sqrt{2\varphi_B - U_{BS}}$$

threshold and $2\varphi_B < \varphi_S$ strong inversion. In modern MOS-devices with thin oxides the carrier concentration in the inversion layer is very high. It is comparable to the quantum states density for electron gas. Since MB approximation is no longer valid it is necessary to take into account the Fermi–Dirac (FD) statistics[3–5]. Using FD distribution for electrons (and MB distribution for the majority carriers—holes) it is straightforward to derive an equation analogous to eqn (2) (following the classic approach for 3-D gas)

$$U_{GS} - V_{FB} - V - \varphi_S = D\left[V + \varphi_S - U_{BS} - U_T + \frac{4U_T}{3\sqrt{\pi}}\exp\left(\frac{E_{c\infty} - E_{i\infty} - \varphi_B}{U_T}\right)F_{3/2}(t_S)\right]^{1/2} \quad (3a)$$

$$t_S = -\frac{E_{c\infty} - E_{i\infty} + \varphi_B - \varphi_S}{U_T} \quad (3b)$$

where $E_{c\infty}$, $E_{i\infty}$ are positive voltage equivalents for conduction band edge and intrinsic level deep in the bulk and $F_{3/2}$ is a Fermi integral of order 3/2.

Charge modeling

The exact model for mobile charge in the inversion layer is given in integral form[6–10], which totally prevents any analytical calculation. In this paper the following approximation is assumed (Q_i is the absolute charge value/cm²):

$$Q_i = C_0(U_{GS} - V_{FB} - V - \varphi_S - D\sqrt{V + \varphi_S - U_{BS} - U_T}). \quad (4)$$

Brews showed in Refs [6,8] that eqn (4) with eqn (2) is a very accurate approximation in weak and strong inversion. It is interesting to investigate the influence of the estimation error of φ_S on the physical quantities in MOSFET in order to know whether we need to use the complex formula (3a,b) in place of eqn (2) in practice. We carried out calculations for the wide intervals of common values for t_{ox}, N_B, U_{GS}, U_{BS} and V. An extreme case is given in Fig. 1. Figure 1(a) shows φ_S vs effective gate voltage ($U_{GSeff} = U_{GS} - U_t$) for MB and FD statistics in the case of a thin oxide:

†With respect to the level φ_B above the quasi-Fermi level for electrons in the inversion layer.

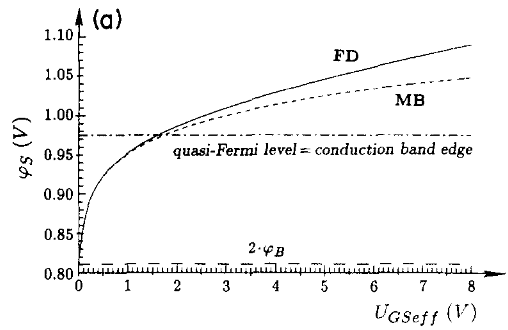

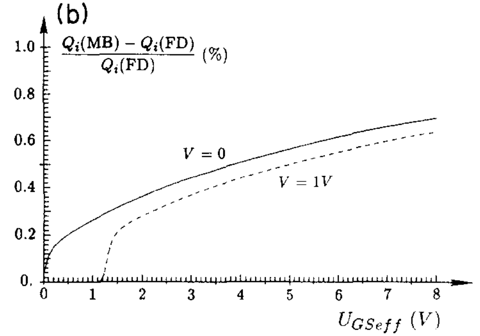

Fig. 1. (a) Relative surface potential calculated using FD eqn (3a,b) and MB eqn (2) statistics vs effective gate voltage. $t_{ox} = 10$ nm, $N_B = 10^{17}$ cm^{-3}, $T = 300$ K, $U_{BS} = 0$, $V = 0$. (b) Percent error in inversion layer charge density per cm² vs effective gate voltage.

$t_{ox} = 10$ nm. Differences arise for $U_{GSeff} > 1$ V. For $U_{GSeff} = 8$ V (oxide breakdown) the difference is about 4%. The corresponding difference in Q_i calculated using eqn (4) with MB and FD statistics is given in Fig. 1(b). This difference is very small in the whole interval of U_{GSeff}. It is comparable to the error of the approximate expression (4) itself[8]. The result can be explained: for a high U_{GSeff}, a small variation in φ_S negligibly alters the value of Q_i. Near and under the threshold ($U_{GSeff} < 1$ V) relative changes of Q_i are very sensitive to small variations in φ_S. However, in this case the differences between MB and FD statistics are negligible for the common oxide thickness. It follows that the model of the charge $Q_i(U_{GS}, U_{BS}, V)$ given by eqns (2) and (4) is accurate enough for practical applications. Consequently, if the carrier degeneracy in the inversion layer is taken into account, the analysis and the calculations carried out in Refs [6,8,11] still hold.

In the analytical modeling of MOSFETs the charge within the depletion region under the gate Q_B is usually calculated using a rectangular approximation of the space-charge density[5,7,9,12–14]. The charge Q_i may then be calculated from the total charge in Si Q_s as:

$$Q_i = Q_s - Q_B = C_o(U_{GS} - V_{FB} - V - \varphi_S - D\sqrt{V + \varphi_S - U_{BS}}) \quad (5)$$

The difference between eqns (4) and (5) is small at the glance, but qualitative. The model (5) coupled with eqn (2) is correct only in strong inversion:

$$U_{GSeff} > 0 \Leftrightarrow \varphi_S > 2\varphi_B \Leftrightarrow Q_i > 0;$$

$$U_{GSeff} = 0 \Leftrightarrow \varphi_S = 2\varphi_B \Leftrightarrow Q_i = 0;$$

$$U_{GSeff} < 0 \Leftrightarrow \varphi_S < 2\varphi_B \Leftrightarrow Q_i < 0$$

(physically meaningless). However, the accurate model (4) gives $Q_i > 0$ for all U_{GSeff} in weak and strong inversion. Assuming the usual approximation $\varphi_S = 2\varphi_B$ from eqn (5) there follows a simple model for the charge Q_i, known from the "book models" of MOSFETs[7,9,15]. For old technologies with thick oxides and high supply voltages U_{GS}, model (5) with $\varphi_S \approx 2\varphi_B$ is satisfying in a considerable part of operating region[9]. However, for modern devices due to thin oxides (<20 nm) and low voltages ($\leqslant 5$ V) this is no longer valid and the φ_S increment above $2\varphi_B$ must be included in analytical MOSFET modeling[5,16]. Comparisons between the accurate model eqn (4) and the approximate model eqn (5) which use a calculated φ_S or $2\varphi_B$ have practical importance. A typical example is given in Fig. 2. Model (5) with φ_S calculated from eqn (2) has a small error in region $U_{GSeff} > 1$ V, while for $U_{GSeff} < 0.2$ V the error is large. The approximation by $2\varphi_B$ leads to a systematic positive error in the charge for $U_{GSeff} > 1$ V (the error is 20% for $U_{GSeff} = 1$ V, $5 \div 10\%$ for 5 V). In the region $U_{GSeff} < 1$ V the approximation by $2\varphi_B$ is poor in case of thin oxide. The calculations carried out for other common values V, N_B, U_{BS} give similar results. It is important to point out that in all above considerations U_t is the theoretical threshold voltage ($\varphi_S = 2\varphi_B$). A threshold voltage determined by a usual linear extrapolation of experimental data is $100 \div 200$ mV higher than the theoretical value[5]. By including this in the model, it can "compensate" the error due to approximation with $2\varphi_B$. In this paper we start from the theoretical threshold voltage. Therefore, the difference $\varphi_S - 2\varphi_B$ shall be taken into account.

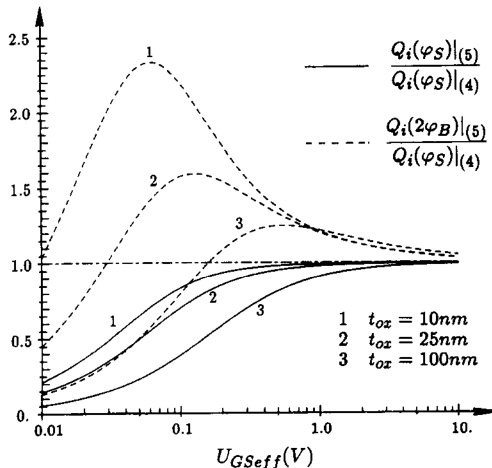

Fig. 2. Ratio of the channel charge density per cm^2 calculated using approximate eqn (5) and "true" formula (4) vs effective gate voltage. φ_S is calculated using eqn (2). $N_B = 10^{17}\,\mathrm{cm}^{-3}$, $T = 300$ K, $V = 0$, $U_{BS} = 0$.

Mobility modeling

We restrict ourselves to room temperature and strong inversion. At first let us discuss the influence of the normal field. The parallel field is low and the carriers are in equilibrium with the lattice (surface ohmic mobility—μ_S). The surface mobility may be expressed in strong inversion as a function of one local quantity—the effective normal field:

$$E_{xeff} = \frac{\gamma Q_i + Q_B}{\epsilon_s} = \frac{\gamma C_o}{\epsilon_s}\left(U_{GS} - V_{FB} - V - \varphi_S + \frac{1-\gamma}{\gamma} D\sqrt{V + \varphi_S - U_{BS} - U_T}\right) \quad (6)$$

The $\mu_S(E_{xeff})$-concept follows necessarily from the quantum carrier distribution in the inversion layer and is well in use in the physical modeling of MOS-devices today[2,16]. The common value for γ is $\frac{1}{2}$[4,17–19]. An approach with general γ allows a proper description of electron and hole mobilities at 77 K and at room temperature[20]. The very first model for μ_S was given by Schrieffer in Ref. [21]. After some approximations this model reduces to (in the effective field concept)

$$\mu_S(E_{xeff}) = \mu_B \Big/ \left(1 + \frac{\mu_B}{a} E_{xeff}\right) \quad (7)$$

where μ_B is the mobility related to surface phonons and a is a parameter for fitting the experimental $\mu_S(E_{xeff})$ data. For high fields the classical model eqn (7) gives: $\mu_S \sim E_{xeff}^{-1}$. However, for high fields (due to quantum broadening of the inversion layer) experimental data show: $\mu_S \sim E_{xeff}^{-\beta}$, $\beta \in (\frac{1}{3}, 1)$[3,4,17,22]. So, eqn (7) predicts a more emphasized decreasing of the surface mobility than the experimental data show. There are a few models in the literature, which describe well the "universal" curve $\mu_S(E_{xeff})$: empirical Yamaguchi's[2,23,24]

$$\mu_S(E_{xeff}) = \frac{\mu_B}{\sqrt{1 + \delta E_{xeff}}} \quad (8)$$

where δ is a fitting parameter; classic-quantum Schwarz–Russek's[17,25]

$$\mu_S(E_{xeff}) = \mu_B \Big/ \left(1 + \frac{\mu_B}{a}\frac{E_{xeff}}{1 + bE_{xeff}^{2/3}}\right) \quad (9)$$

with fitting parameters a, b and other models[4,19]. Experiments show that $\mu_S(E_{xeff})$ is a reproducible characteristic in strong inversion (Figs 3 and 4), independent of the oxide thickness[3,5,19]. The characteristic $\mu_S(E_{xeff})$ is weakly dependent on the bulk doping due to screening of the ionized impurities (the carrier concentrations are very high in the inversion layer)[18]. Therefore, the reduction of μ_B due to scattering caused by the bulk impurity ions (often

taken into account in numerical simulations of MOS-devices[23,25–27]) is not appropriate for the description of the inversion layer. The influence of the fixed oxide charge (and interface trapped charge) on μ_S, modeled in Ref. [17] (empirically in Ref. [18]), is important for high-quality technologies only at small U_{GSeff} and in subthreshold region. It will not be taken into account here (the prerequisite for eqn (9)). We propose a new parameter set for the presented models in (100) surface at 300 K: electrons $\mu_{Bn} = 1100\,cm^2/Vs$ (close to values given in Refs [4,17,27,28]), holes $\mu_{Bp} = 355\,cm^2/Vs$. For Yamaguchi's eqn (8)

$$\delta_n = 1.45 \times 10^{-5}\,cm/V,$$

$$\delta_p = 3.2 \times 10^{-5}\,cm/V.$$

For Schwarz–Russek's eqn (9)

$$a_n = 8.6 \times 10^7\,cm/s,$$

$$b_n = 4.47 \times 10^{-4}(cm/V)^{2/3},$$

$$a_p = 1.3 \times 10^7\,cm/s,$$

$$b_p = 5.7 \times 10^{-4}(cm/V)^{2/3}.$$

Comparisons between eqns (7), (8), (9) and several experimental data from the literature are made in Figs 3 and 4. The classical model eqn (7) agrees with experiments at lower E_{xeff}, which gives $a_n = 2.3 \times 10^8\,cm/s$, $a_p = 4.2 \times 10^7\,cm/s$, while at higher E_{xeff} a functional discrepancy occurs. Models (8) and (9) agree well with experimental data.

The inversion layer mobility is usually modeled at simultaneous high normal and parallel fields starting from some bulk mobility model $\mu(\mu_o, E_y, v_{sat})$ where E_y is the field in the current direction, μ_o is the ohmic mobility and v_{sat} is the saturation velocity. Hence, μ_o is replaced by the ohmic mobility in the inversion layer $\mu_S(E_{xeff})$:

$$v_d(E_{xeff}, E_y) = \mu(\mu_S(E_{xeff}), E_y, v_{sat}) \cdot E_y. \quad (10)$$

Such approach is widely in use for analytical[2,12,29] and numerical[23,25–27] MOSFET modeling. It has

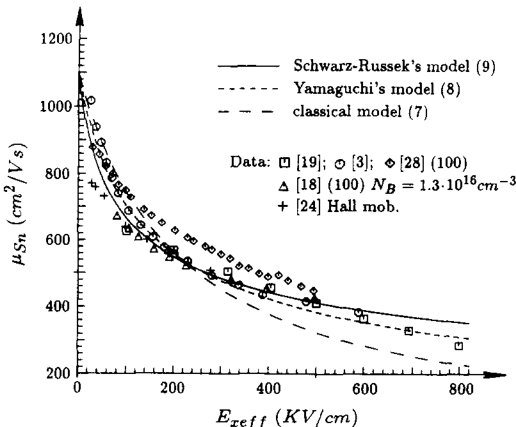

Fig. 3. Comparison between calculated electron surface ohmic mobility and experimental data.

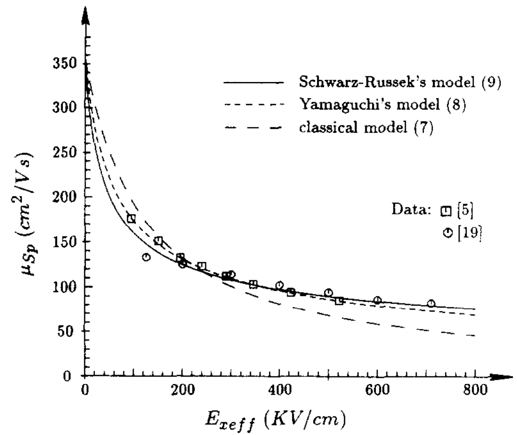

Fig. 4. Comparison between calculated hole suface ohmic mobility and experimental data.

a correct asymptotic behaviour: at low E_y follows $\mu \to \mu_S(E_{xeff})$—the condition for the measurement of μ_S; at high E_y follows $v_d \to v_{sat}$, independent of E_{xeff}. However, there exists no evidence for the correctness of such approach at medium E_y fields. In this paper we shall discuss the hyperbolic model[2,12,30]

$$v_d = \left\{\mu_S(E_{xeff}) \middle/ \left[1 + \frac{\mu_S(E_{xeff})}{v_{sat}} \cdot E_y\right]\right\} \cdot E_y \quad (11)$$

and the model proposed by Jaggi in the form (10)

$$v_d = \left\{[2 \cdot \mu_S(E_{xeff})] \middle/ \left[1 + \sqrt{1 + \left(\frac{2\mu_S(E_{xeff})E_y}{v_{sat}}\right)^2}\right]\right\} \cdot E_y \quad (12)$$

Jaggi's model is derived theoretically for bulk Si ([26] and Refs therein) and agrees well with the experimental data for bulk Si in directions ⟨111⟩ or ⟨110⟩ at room temperature[22]. We shall examine eqn (10) for hyperbolic and Jaggi's model by comparing with the $v_d(E_{xeff}, E_y)$ experimental data given in Ref. [28]—Fig. 5. For μ_S the model (8) is assumed with parameters given above. There are discussions about the value for v_{sat} in the inversion layer[23,28,31]. At very high E_y the carriers have a large average energy and the inversion layer becomes broad—population of higher (wider) subbands occurs. The carriers interact more with bulk-phonons than with surface-phonons. Consequently, we assume a value for bulk Si: $v_{satn} = 1.04 \times 10^7\,cm/s$. At low E_y (2.6 kV/cm) the model (12) predicts well v_d, because μ_S is appropriate (Fig. 3). At high fields (41.6 kV/cm) eqn (12) agrees with experimental v_d, which suggests a proper choice of v_{satn}. At medium fields the experimental v_d is higher than calculated (for eqn (12) the error is 8% at $E_y = 10.4\,kV/cm$). A proper explanation is carrier heating due to E_y[17]. The inversion layer becomes broader, μ_S increases and v_d increases too. It follows that the form (10) is not correct. A better physical approach is to put $\mu_S[E_{xeff}, T_e(E_y)]$ in place of $\mu_S(E_{xeff})$, where T_e is the carrier "temperature". However, we believe Jaggi's model (12) describes the

electron mobility in the inversion layer accurately enough for analytical modeling (max error < 10%). For the hyperbolic model (11) the error is larger, because the error due to "soft saturation" is added to the error due to carrier heating ($E_y = 10.4$ kV/cm, $25 \div 30\%$). The hyperbolic model is inappropriate for electrons, but we believe it is accurate enough for holes[26]. Consequently eqn (12) will be used for N-channel devices, while eqn (11) for P-channel devices. Note, in Refs [17] and [28] a good fitting of the experimental $v_d(E_{xeff}, E_y)$ data used above was given, but using those models does not enable an analytical calculation of the drain current. However, Jaggi's model (12) makes this possible (Section 3).

Formulation of the current equations

There are two equivalent approaches to the calculation of the current density: either as a sum of a drift and a diffusion component or using a quasi-Fermi level. Using the first approach the drain current may be expressed in the quasi-1-D-formulation as [11,14,32]

$$I_D = -W\mu(E_{xeff}, E_y)Q_i E_y - WD(E_{xeff}, E_y)\frac{\partial Q_i}{\partial y} \quad (13)$$

and using the second as[6]

$$I_D = W\mu(E_{xeff}, E_y)Q_i\frac{\partial V}{\partial y} \quad (14)$$

where W is a channel width and D is a diffusion coefficient. The parallel field at the surface is: $E_y = -\partial V/\partial y \cdot (1 + \partial\varphi_S/\partial V)$ (the surface potential for the reference level $E_{i\infty}$ is $V + \varphi_S - U_{BS}$). The approaches (13) and (14) are generally not equivalent,

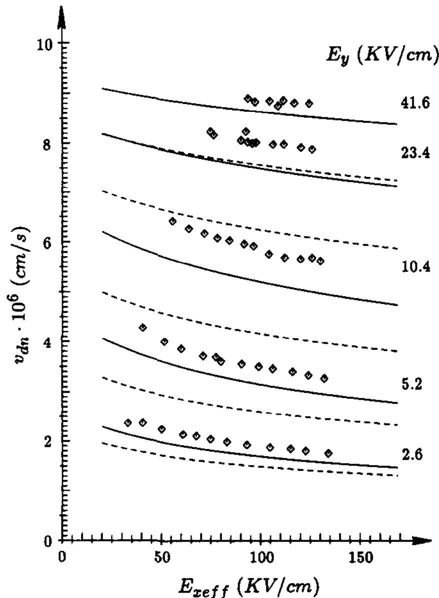

Fig. 5. Comparison between calculated drift and experimental data given by Cooper and Nelson[28] (◇), 300 K, surface (100), direction [011]. Jaggi's model eqn (12) ——; hyperbolic model eqn (11) – – –.

dependent on the models for Q_i and φ_S. In this paper φ_S is determined by the solution of Poisson's equation (2), while Q_i is given empirically by eqn (4). The relative difference between currents in eqns (13) and (14) may be obtained analytically as: $\partial\varphi_S/\partial V - U_T/Q_i \cdot \partial Q_i/\partial V$. For the model (4) with eqn (2) the numerical calculations have shown that this difference is small in strong inversion. It vanishes in the deep subthreshold region. For the model (5) with eqn (2) the difference is large in the region $U_{GSeff} < 1$ V[22]. In the formulation proposed in Ref. [6]: $\varphi_S(V = 0)$ is determined by eqn (2), while $Q_i(\varphi_S, V)$ and $\varphi_S(V > 0)$ are given by eqn (4) and with the condition that eqn (13) is identical to eqn (14). This approach differs slightly from ours in practice. The model (14) has a simpler form than eqn (13) and will therefore be used henceforward. Using driving force instead of E_y in the expressions for the mobility degradation due to parallel field is a physically better approach[26]. As we neglect carrier heating the driving force is reduced to the gradient of the quasi-Fermi level, $\partial V/\partial y$. Hence, eqn (14) is used with $\mu(E_{xeff}, E_y)$ replaced by $\mu(E_{xeff}, \partial V/\partial y)$. This substitution simplifies eqn (14) considerably. The boundary conditions are

$$V(0) = 0; \quad V(L_{eff}) = U_{DS} \quad (15)$$

where L_{eff} is an effective channel length. The potential difference between the source and the drain channel end is $\varphi_S(L_{eff}) - \varphi_S(0) + U_{DS}$, which differs from U_{DS} (discussed in detail in Ref. [6]). Although eqn (14) has the well known drift form at a glance, the system (2)(4)(14)(15) assumes both drift and diffusion current components and is valid both in weak and strong inversion. Note that, assuming a deep subthreshold operation point, after some approximation, it can be reduced to the well known long-channel subthreshold current expression[7,15].

3. DRAIN CURRENT IN THE TRIODE REGION

The current in the triode region is determined by system of eqns (2)(4)(14), boundary conditions (15) and mobility models (11) or (12), with μ_S given by eqns (7), (8) or (9).

Hyperbolic mobility model

Replacing eqn (11) for μ in eqn (14) (with E_y replaced by $\partial V/\partial y$), after integration and using eqn (15) we obtain

$$I_D = \frac{WC_o\mu_B}{L_{eff}} \frac{I_1}{1 + [\mu_B/(v_{sat}L_{eff})]I_2} \quad (16)$$

where

$$I_1 = \int_0^{U_{DS}} \frac{\mu_S(E_{xeff})}{\mu_B} \frac{Q_i(V + \varphi_S(V))}{C_o} dV \quad (17)$$

$$I_2 = \int_0^{U_{DS}} \frac{\mu_S(E_{xeff})}{\mu_B} dV \quad (18)$$

In eqn (17) Q_i is given by eqn (4). The integrals (17) and (18) are generally not solvable. This has been overcome usually by taking μ_S out of the integral and using an "average" μ_S dependent on terminal voltages[1,12,29,33,34]. Using the local classical model (7) with E_x at the surface a closed solution of the integral (17) may be obtained[13,30,35,36]. The local models in the effective field concept are applied in novel papers: the classic model (7) in Refs [16,37,38], Yamaguchi's expression (8) (approximately) in Ref. [2]. In this paper a novel approach is proposed based on the polynomial expansion:

$$\mu_S[E_{x\text{eff}}(V)] = \sum_{i=0}^{\infty} \frac{(V - V^*)^i}{i!} \frac{\partial^i \mu_S}{\partial V^i}\bigg|_{V^*} \quad (19)$$

V^* depends solely on the supply voltages U_{GS}, U_{BS}, U_{DS}. The function $\mu_S(E_{x\text{eff}})$ is slowly decreasing (in strong inversion at room temperature—Figs 3 and 4) and $E_{x\text{eff}}$ is a slowly varying function of V (eqn (6)). Consequently we expect a good approximation of $\mu_S(V)$ by taking a few first terms of the expansion (19). φ_S is usually approximated by $2\varphi_B$. In accordance with the considerations in Section 2 hence $\varphi_S - 2\varphi_B$ is taken into account. The change of φ_S with y is not regarded. φ_S is "averaged" along the channel in the following manner: we calculate φ_S at a point $V = \eta \cdot U_{DS}$, where $\eta \in [0, 1]$ and denote it as φ_S^η. A constant φ_S along the channel is assumed that equals to φ_S^η. From eqn (2) an equation for φ_S^η follows:

$$U_{GS} - V_{FB} - \eta U_{DS} - \varphi_S^\eta = D\left[\eta U_{DS} + \varphi_S^\eta - U_{BS} - U_T + U_T \exp\left(\frac{\varphi_S^\eta - 2\varphi_B}{U_T}\right)\right]^{1/2} \quad (20)$$

φ_S^η depends on U_{GS}, U_{DS}, U_{BS}, but not on V. The local potential $\varphi_S(y)$ decreases monotonically from source to drain (Appendix A). Consequently, by putting φ_S^η in the place of $\varphi_S(y)$ the potential φ_S is underestimated near the source and overestimated near the drain. For Q_i the opposite is valid. These opposite errors partially compensate each other by integration of eqn (17). Using $\varphi_S = \varphi_S^\eta$ and the series (19) reduces eqn (17) to:

$$I_1 = \sum_{i=0}^{\infty} \frac{\partial^i(\mu_S/\mu_B)}{i!\,\partial V^i}\bigg|_{V_1^*} \sum_{k=0}^{i} \binom{i}{k} (-1)^{i-k} V_1^{*\,i-k} J_k \quad (21)$$

where V_1^* is an appropriate point for I_1. The integrals J_k are given by:

$$J_k = \int_0^{U_{DS}} V^k (U_{GS} - V_{FB} - \varphi_S^\eta - V - D\sqrt{V + \varphi_S^\eta - U_{BS} - U_T})\,dV \quad (22)$$

For I_2 there follows:

$$I_2 = \sum_{i=0}^{\infty} \frac{\partial^i(\mu_S/\mu_B)}{i!\,\partial V^i}\bigg|_{V_2^*} \int_0^{U_{DS}} (V - V_2^*)^i\,dV. \quad (23)$$

The terms $\partial^i\mu_S/\partial V^i$ can analytically be calculated for any explicit $\mu_S(E_{x\text{eff}})$ model. J_k are integrals of an algebraic integrand and are easily solvable. Therefore I_1, I_2 and finally I_D can analytically be expressed to any desired accuracy. The derivatives and integrals of higher order in eqns (21) and (23) are very complex. Our aim is to express I_1 and I_2 sufficiently accurate using a minimal number of terms in the series. Taking the first two terms yields:

$$I_1 \approx \frac{\mu_S(V_1^*)}{\mu_B} J_0 + \frac{\partial \mu_S}{\mu_B\,\partial V}\bigg|_{V_1^*} (J_1 - V_1^* J_0) \quad (24)$$

$$I_2 \approx \frac{\mu_S(V_2^*)}{\mu_B} U_{DS} + \frac{\partial \mu_S}{\mu_B\,\partial V}\bigg|_{V_2^*} U_{DS}\left(\frac{U_{DS}}{2} - V_2^*\right). \quad (25)$$

The mean-value theorem for integrals ensures the existence of V_1^*, V_2^* for which: $I_1 = \mu_S(V_1^*)J_0/\mu_B$; $I_2 = \mu_S(V_2^*)U_{DS}/\mu_B$. These optimal points cannot be determined practically. We choose these points thus the simplest form of the final expression is obtained, namely the coefficients of the first derivative will be eliminated:

$$V_1^* = \frac{J_1}{J_0};\quad V_2^* = \frac{U_{DS}}{2}. \quad (26)$$

The error in the current due to the approximations of I_1 and I_2 may be investigated only numerically. The current was calculated analytically by eqn (16) using the first two (eqns (24), (25)) or three terms in the series. Exact values where obtained by eqn (16) using numerical integration of (17) and (18). By integration a corresponding $\varphi_S(V_k)$ was calculated at each discrete point $V_k \in [0, U_{DS}]$ [from eqn (2)]. The error in the analytical current model results from:

—the approximation: $\varphi_S(V) = \varphi_S^\eta$
—truncation of the series in eqns (21) and (23)

The error analysis was carried out in the whole triode region (in its linear part and at the boundary towards the saturation region) and L_{eff}, t_{ox}, N_B were varied in large intervals. This error analysis shows that the dominant error is due to the approximation $\varphi_S = \varphi_S^\eta$. By a fixed η the differences between relative errors in I_1, I_2 and currents calculated using two and three terms are at least one order less than the errors themselves. Namely, by taking the third terms the change in relative error was 0.5% max. On the other hand the error in I_1, I_2 and current depend significantly on η. Therefore it is enough to take only the first two terms—linear local approximation—eqns

(24) and (25). By choice (26) the simplest expression for I_D is obtained:

$$I_D = \frac{WC_o}{L_{eff}}\left\{[\mu_S[E_{xeff}(V_1^*, \varphi_S^\eta)]J_0] \Big/ \left[1 + \frac{\mu_S[E_{xeff}(V_2^*, \varphi_S^\eta)]}{v_{sat} L_{eff}} U_{DS}\right]\right\} \tag{27a}$$

$$V_1^* = \left.\frac{J_1}{J_0}\right|_{U_{DS}\neq 0}; \quad V_2^* = \frac{U_{DS}}{2} \tag{27b}$$

$$J_0 = (U_{GS} - V_{FB} - \varphi_S^\eta)U_{DS} - \frac{U_{DS}^2}{2} - \tfrac{2}{3}D[(U_{DS} + \varphi_S^\eta - U_{BS} - U_T)^{3/2} - (\varphi_S^\eta - U_{BS} - U_T)^{3/2}] \tag{27c}$$

$$J_1 = (U_{GS} - V_{FB} - \varphi_S^\eta)\frac{U_{DS}^2}{2} - \frac{U_{DS}^3}{3} - 2D \times \left[\frac{(U_{DS} + \varphi_S^\eta - U_{BS} - U_T)^{5/2} - (\varphi_S^\eta - U_{BS} - U_T)^{5/2}}{5}\right.$$
$$\left. - (\varphi_S^\eta - U_{BS} - U_T)\frac{(U_{DS} + \varphi_S^\eta - U_{BS} - U_T)^{3/2} - (\varphi_S^\eta - U_{BS} - U_T)^{3/2}}{3}\right] \tag{27d}$$

For $U_{DS} = 0$, $I_D = 0$ holds. In eqn (27a) $E_{xeff}(V_{1,2}^*, \varphi_S^\eta)$ are given by eqn (6).

Because of $V_1^* \in [0, U_{DS}/2]$ both points V_1^*, V_2^* are some midpoints in the channel. Actually, we have "averaged" μ_S along the channel. The derived model eqn (27a) has a form that is equivalent to the present models in literature, which assume the hyperbolic mobility model and some surface mobility model dependent on terminal voltages with empirical parameters[12]. However, our expression is derived: using a local linear approximation of $\mu_S[E_{xeff}(V)]$ in the integration interval, checking the error due to truncation of the power expansion and eliminating the first derivative term. Note that $\mu_S(E_{xeff})$ in eqn (27a) may be any physical, temperature dependent, local model for the surface mobility.

The substitution of $\varphi_S(V)$ by a constant $\varphi_S^\eta(U_{DS})$ changes the qualitative behaviours of the Q_i model. The detailed explanations are given in Appendix A. Here we point out that an η in the interval $0 \leqslant \eta < 1$ yields a finite U_{DSsc} and $Q_i(V) > 0$ is ensured for all U_{DS}: $0 \leqslant V \leqslant U_{DS} < U_{DSsc}$, where U_{DSsc} is the classical saturation voltage (defined by $Q_i(U_{DSsc}) = 0$ – [7, 9]). For $\eta = 1$ a finite U_{DSsc} does not exist and $Q_i(V) > 0$ holds for all $V \geqslant 0$. An important consequence is that J_k are positive in the triode region for all η. Note that the triode region is defined with $0 \leqslant U_{DS} \leqslant U_{DSs} < U_{DSsc}$; $U_{GS} \geqslant U_t$, where U_{DSs} is the short-channel saturation voltage. Let us now discuss the influence of η on the error in the current. Figure 6(a) shows the current at the saturation point calculated numerically and analytically with $2\varphi_B$, $\eta = 0.0, 0.5$ and 1.0. The boundary between the triode and the saturation region is chosen for the comparison, because of the highest change of $\varphi_S(y)$ along the channel (for the calculation of saturation point see comments in Section 4). The corresponding errors in current are given in Fig. 6(b). An obviously "optimal" choice is $\eta = 0.5$, which gives a very small error for $U_{GSeff} > 0.3$ V. For $\eta = 0$, φ_S is overestimated,

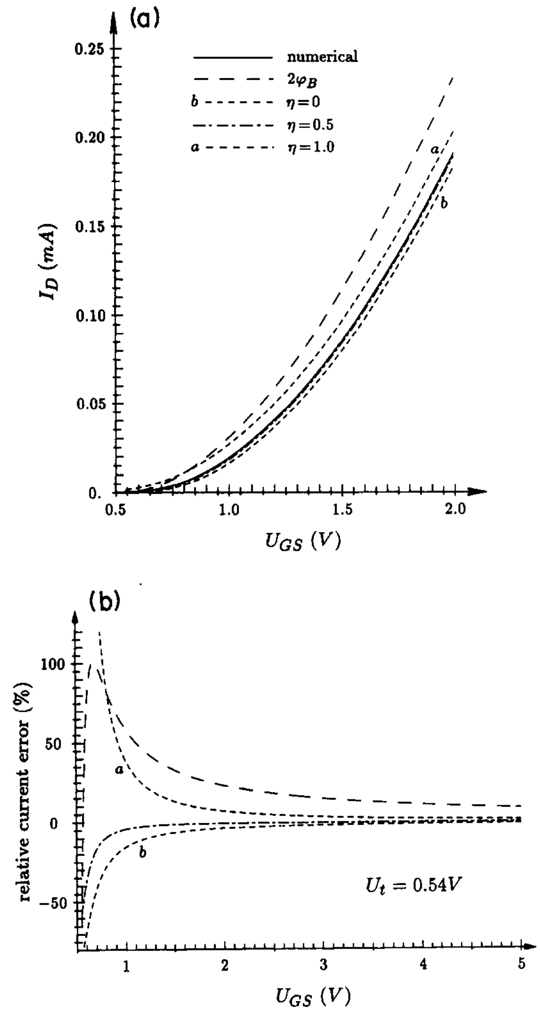

Fig. 6. (a) Comparison between numerical and analytical current at the saturation point. Model: hyperbolic and eqn (9), N-channel MOSFET: $L_{eff} = 2\,\mu$m, $t_{ox} = 20$ nm, $W = 8\,\mu$m, $N_B = 5 \times 10^{16}$ cm^{-3}, $V_{FB} = -0.9$ V, 300 K, $U_{BS} = 0$ V. (b) Percent error in analytically calculated current.

while Q_i and finally I_D are underestimated. At $\eta = 1$ the opposite is valid. Using $2\varphi_B$ the charge Q_i and therefore I_D are significantly overestimated (similar as in Fig. 2). We see that using φ_S^η the model becomes more accurate than in the case with $2\varphi_B$, but it becomes necessary to solve the transcendental eqn (20). However, this equation can be solved with precision 0.1% in $3 \div 6$ iterations[22].

We propose the model (27a–d) for P-channel MOSFETs (with appropriate changes in sign of current and potentials).

Jaggi's mobility model

The hyperbolic expression (11) is not quantitatively proper for the inversion layer mobility of electrons—Fig. 5. A better description is given by a square-root formula[34]. Due to difficulty to solve the corresponding integral this model was used approximately and empirically[1,35]. Strictly speaking, by the charge model (4) or (5), the square-root model leads to elliptic integrals, which are not solvable in closed form. The models applied in Refs [34] and [39] are also proper for electrons. They enable an analytical solution of the corresponding integrals. However, they lead to implicit equations for the current in the triode region. Jaggi's model (12) describes the drift of electrons in the inversion layer properly—Fig. 5. It was used up to now only for numerical simulations (for example MINIMOS 3[26], 4 and 5). It leads to an explicit analytical expression for the drain current as shall be shown below. Substituting eqn (12) into eqn (14) (with E_y replaced by $\partial V/\partial y$) we obtain a square equation for I_D after one integration using eqn (15). The physical solution is:

$$I_D = \frac{WC_o\mu_B}{L_{eff}}\left\{2I_1\bigg/\left[1 + \sqrt{1 + \left(\frac{2\mu_B}{v_{sat}L_{eff}}\right)^2 I_1 I_3}\right]\right\} \quad (28)$$

where I_1 is given by eqn (17) and I_3 by

$$I_3 = \int_0^{U_{DS}} \frac{\mu_S(E_{xeff})/\mu_B}{Q_i[V + \varphi_S(V)]/C_o}\,dV \quad (29)$$

Similarly as for the hyperbolic model henceforward μ_S is substituted by eqn (19) and $\varphi_S(V)$ by φ_S^η. For I_1 there follows eqn (21) and the approximation (24). For I_3 an expression analogous to eqn (21) is obtained, with a characteristic point V_3^* (in the place of V_1^*) and the integrals

$$\mathscr{F}_k = \int_0^{U_{DS}} \frac{V^k}{U_{GS} - V_{FB} - \varphi_S^\eta - V - D\sqrt{V + \varphi_S^\eta - U_{BS} - U_T}}\,dV \quad (30)$$

(in the place of J_k). The integrals $\mathscr{F}_k$ are solvable in closed form. I_3 and finally I_D can analytically be calculated to any desired accuracy. The error analysis has been carried out equivalently as for the hyperbolic model and gives similar results. Third and higher terms in expansions have a negligible influence on error in current. The error depends directly on η. Therefore the first two terms in the expansion of I_3 shall be taken:

$$I_3 \approx \frac{\mu_S(V_3^*)}{\mu_B}\mathscr{F}_0 + \left.\frac{\partial\mu_S}{\mu_B\,\partial V}\right|_{V_3^*}(\mathscr{F}_1 - V_3^*\mathscr{F}_0) \quad (31)$$

V_1^* and V_3^* are chosen such that the coefficients of the first derivatives vanish:

$$V_1^* = \frac{J_1}{J_0};\quad V_3^* = \frac{\mathscr{F}_1}{\mathscr{F}_0} \quad (32)$$

Finally, for N-channel MOSFET, for $U_{DS} \neq 0$, I_D is given by eqn (28) and:

$$I_1 = \frac{\mu_S(V_1^*, \varphi_S^\eta)}{\mu_B}J_0;\quad I_3 = \frac{\mu_S(V_3^*, \varphi_S^\eta)}{\mu_B}\mathscr{F}_0 \quad (33a)$$

where V_1^*, V_3^* are given by eqn (32), J_0, J_1 by (27c,d) and $\mathscr{F}_0, \mathscr{F}_1$ are

$$\mathscr{F}_0 = \frac{2}{\sqrt{D^2 + 4A}}(x_1 B_1 - x_2 B_2) \quad (33b)$$

$$\mathscr{F}_1 = -U_{DS} + 2D(\sqrt{U_{DS} + \varphi_S^\eta - U_{BS} - U_T} - \sqrt{\varphi_S^\eta - U_{BS} - U_T}) - 2EB_1 - 2FB_2 \quad (33c)$$

where

$$A = U_{GS} - V_{FB} - U_{BS} - U_T \quad (33d)$$

$$x_1 = -\frac{D + \sqrt{D^2 + 4A}}{2};\quad x_2 = \frac{\sqrt{D^2 + 4A} - D}{2} \quad (33e)$$

$$B_1 = \ln\frac{\sqrt{U_{DS} + \varphi_S^\eta - U_{BS} - U_T} - x_1}{\sqrt{\varphi_S^\eta - U_{BS} - U_T} - x_1} \quad (33f)$$

$$B_2 = \ln\frac{x_2 - \sqrt{U_{DS} + \varphi_S^\eta - U_{BS} - U_T}}{x_2 - \sqrt{\varphi_S^\eta - U_{BS} - U_T}} \quad (33g)$$

$$E = \frac{AD - x_1(U_{GS} - V_{FB} + D^2 - \varphi_S^\eta)}{\sqrt{D^2 + 4A}} \quad (33h)$$

$$F = \frac{x_2(U_{GS} - V_{FB} + D^2 - \varphi_S^\eta) - AD}{\sqrt{D^2 + 4A}} \quad (33i)$$

For $U_{DS} = 0$, $I_D = 0$ holds.

For $\eta < 1$ a finite U_{DSsc} exists (Appendix A). A limitation $U_{DS} < U_{DSsc}$ ensures that $Q_i > 0$ holds. For $\eta = 1$ a finite U_{DSsc} does not exist and $Q_i > 0$ holds for all U_{DS}. Consequently the proposed model is physically reasonable and the obtained final functions (32), (33a–i) (logarithms and square roots) are defined for all U_{DS} in the triode region and for all η. The

parameter η affects the error in current similarly as for the hyperbolic model. I_3 is found to be more sensitive to η than I_1. However, for large U_{DS}, where I_3 is important, the approximation of I_3 is good, which results in a small error in current. Figure 7(a) shows the comparisons between output characteristics in the triode region calculated numerically and analytically by eqns (28), (27c,d), (32), (33a–i). The corresponding errors are shown in Fig. 7(b). The error in the analytical model with φ_S^{ξ} vanishes for a small U_{DS} due to small changes in $\varphi_S(y)$ along the channel. An *a priori* best choice for η is 0.5. We believe $\eta = 0$ yields a satisfactory accuracy in practice. Note that for $\eta = 0$, φ_S^{ξ} is independent of U_{DS}. In order to calculate the output characteristics for a given U_{GS} it is necessary to solve then the eqn (20) only one time. For $\eta > 0$, φ_S^{ξ} depends on U_{DS} and we need to solve eqn (20) at each operating point.

$V_3^* \in [U_{DS}/2, U_{DS}]$ holds. Therefore V_1^*, V_3^* are some midpoints in the channel. The derived model for the current is a bit more complex than the present models in literature, but it is explicit:

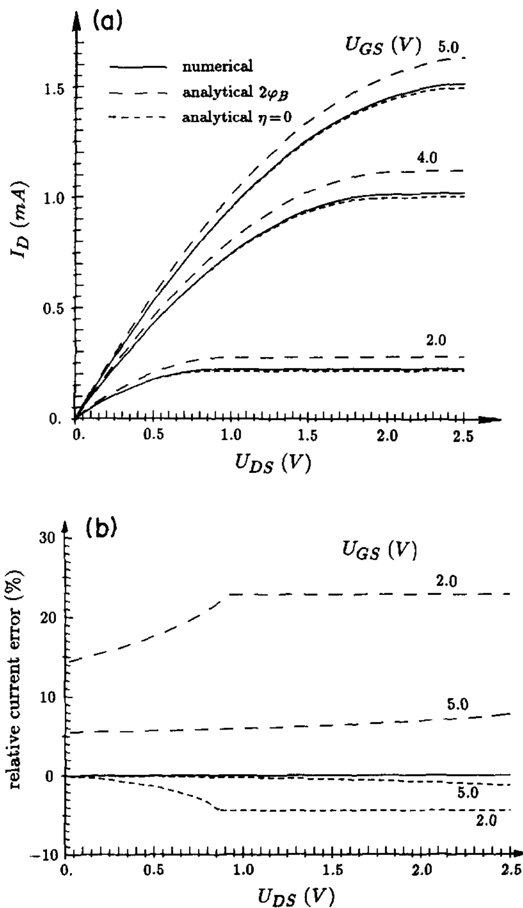

Fig. 7. (a) Output characteristics calculated numerically and analytically. Model: Jaggi's and eqn (8). Parameters for MOSFET are the same as for Fig. 6. (b) Percent error in analytical current.

$I_D(U_{GS}, U_{BS}, U_{DS})$. It can effectively and simply be implemented in computer simulations because it demands only the calculation of 4 square roots and 2 logarithms per bias point.

4. THE EXTENSIONS OF THE MODEL

For the proposed models (Jaggi's and hyperbolic) a differentiable extension into the saturation region is derived[22]. The extension is based on the continuity of $g_d = \partial I_D/\partial U_{DS}$ at the boundary between the triode and saturation region. g_d may easily be calculated analytically because $\partial J_k/\partial U_{DS}$ and $\partial \mathscr{F}_k/\partial U_{DS}$ follow from eqns (22) and (30) directly. However, it is necessary to calculate analytically $\partial \mu_S(E_{xeff})/\partial V$ also. For $\eta = 0$ the short-channel saturation voltage U_{DSs} is determined by a solution of an implicit equation (φ_S^{ξ} depends solely on U_{GS}). For $\eta > 0$ the previous equation is coupled with eqn (20), which forms a system of two implicit equations (φ_S^{ξ} depends on U_{DSs}). The developed iterative solution procedures can solve these equations in a reasonable short computer time, especially for $\eta = 0$.

A differentiable extension into subthreshold region is necessary in a complete modeling of VLSI MOSFETs. Our starting system of equations is valid in weak inversion (Section 2), but the final derived current models are not valid (see Fig. 6b). An explanation is our approximation of a constant φ_S, because the variation of φ_S along the channel is just important in subthreshold region. Using an expansion of μ_S with respect to $\varphi_S + V$, a variable $\varphi_S(V)$ [given with eqn (2)] may be taken into account. The corresponding integrals are solvable in a closed form. A unique expression for the current should be obtained in subthreshold and triode region. The final expressions are complex and will not be presented here.

The 2-D and 3-D effects due to source, drain and gate depletion regions (narrow and inverse-narrow effect and charge sharing) may be included in our model as an empirical correction of the body factor D[7,12,15,37]. D becomes a function of supply voltages and some geometrical-technological parameters. The drain-induced-barrier-lowering effect may be modeled approximately as a correction of the channel length L_{eff}[7,15].

A homogeneously doped bulk, which is a starting assumption in our model, is an invalid approximation for modern MOS-devices with multiple-implanted bulk. It is necessary to improve the eqn (2) and the expression for Q_B in eqns (4) and (6). In addition a new value for V_{FB} and a new inversion criterion ($2\varphi_B$) must be introduced. Using a box-approximation of the doping profile (along the x-axis)[7] it is possible to carry out the procedure given in Section 3 and to obtain an explicit drain current expression. A doping profile transformation proposed in Refs [37,15] is applicable too.

5. SUMMARY AND CONCLUSION

In this paper we start from the fact that for modern technologies the inversion layer mobility is a reproducible characteristic for the (100) surface at room temperature, which can *a priori* be modeled accurately using the expressions given in Section 2. Taking into account the accurate models for the inversion layer mobility (at simultaneous high normal and parallel fields) and the charge, a physics based system of equations for quasi-1-D-modeling of MOSFETs is obtained (Section 2). An approximate, but accurate, analytical solution of this system is derived in the triode region (Section 3). The derived drain current model is explicit and suitable for computer simulations. The proposed current model:

(1) Takes into account complex, highly accurate, modeling of $\mu_S(E_{xeff})$, without inclusion of any unknown empirical parameter,

(2) Is based on a hyperbolic mobility model for P-channel and Jaggi's model for N-channel MOSFETs,

(3) Takes into account approximately the difference $\varphi_S - 2\varphi_B$,

(4) Has the temperature dependence defined by the mobility ($\mu_B, \delta, a, b, v_{sat}$) and other physical parameters (U_T, φ_B, V_{FB}). Appropriate temperature dependence of parameters are given in Refs [7,17,22].

Because of (4), the model is especially applicable for fast simulation of the influences of ambient temperature on static MOSFETs characteristics, or for coupled electrical–thermal (non-isothermal) simulation of MOSFETs characteristics. The further extensions of the model lead towards realistic modeling of VLSI MOSFETs (Section 4). The proposed approach can be a way to reduce the number of unknown fitting parameters in predictive analytical MOSFET modeling.

Acknowledgements—I have pleasure to thank Professors V. Cvekić, D. Tjapkin, S. Selberherr and H. Pötzl for many stimulating discussions and their encouragement. I am grateful to Digital Equipment Corporation at Hudson, U.S.A., for supporting my work.

REFERENCES

1. T. Grotjohn and B. Höfflinger, *IEEE Trans. Electron Devices* **ED-31,** 234 (1984).
2. S.-W. Lee and R. C. Rennick, *IEEE Trans. CAD* **7,** 952 (1988).
3. G. Baccarani and M. R. Wordeman, *IEEE Trans. Electron Devices* **ED-30,** 1295 (1983).
4. A. Rothwarf, *IEEE Electron Device Lett.* **EDL-8,** 499 (1987).
5. B. Majkusiak and A. Jakubowski, *IEEE Trans. Electron Devices* **ED-33,** 1717 (1986).
6. J. R. Brews, *Solid-St. Electron.* **21,** 345 (1978).
7. S. M. Sze, *Physics of Semiconductor Devices*, 2nd edn. Wiley, New York (1981).
8. J. R. Brews, *IEEE Trans. Electron Devices* **ED-33,** 182 (1986).
9. R. S. C. Cobbold, *Theory and Applications of Field-Effect Transistors.* Wiley, New York (1970).
10. H. C. Pao and C. T. Sah, *Solid-St. Electron.* **9,** 927 (1966).
11. L. M. Dang, *Solid-St. Electron.* **20,** 781 (1977).
12. L. M. Dang, *IEEE J. Solid-St. Circuits* **SC-14,** 358 (1979).
13. G. Baccarani, F. Landini and B. Riccó, *IEE Proc.* **127,** 62 (1980).
14. H.-K. Lim and J. G. Fossum, *IEEE Trans. Electron Devices* **ED-30,** 713 (1983).
15. D. K. Ferry, L. A. Akers and E. W. Greeneich, *Ultra Large Scale Integrated Microelectronics.* Prentice-Hall, Englewood Cliffs (1988).
16. T. J. Krutsick, M. H. White, H.-S. Wong and R. V. H. Booth, *IEEE Trans. Electron Devices* **ED-34,** 1676 (1987).
17. S. A. Schwarz and S. E. Russek, *IEEE Trans. Electron Devices* **ED-30,** 1634 (1983).
18. S. C. Sun and J. D. Plummer, *IEEE Trans. Electron Devices* **ED-27,** 1497 (1980).
19. M.-S. Liang, J. Y. Choi, P.-K. Ko and C. Hu, *IEEE Trans. Electron Devices* **ED-33,** 409 (1986).
20. N. D. Arora and G. S. Gildenblat, *IEEE Trans. Electron Devices* **ED-34,** 89 (1987).
21. J. R. Schrieffer, *Phys. Rev.* **97,** 641 (1955).
22. P. Habaš, Thesis, University of Beograd Yug (1989).
23. K. Yamaguchi, *IEEE Trans. Electron Devices* **ED-30,** 658 (1983).
24. M. Tanimoto and D. K. Ferry, *IEEE Electron Device Lett.* **EDL-4,** 246 (1983).
25. A. Hiroki, S. Odanaka, K. Ohe and H. Esaki, *IEEE Electron Device Lett.* **EDL-8,** 231 (1987).
26. W. Hänsch and S. Selberherr, *IEEE Trans. Electron Devices* **ED-34,** 1074 (1987).
27. T. Nishida and C.-T. Sah, *IEEE Trans. Electron Devices* **ED-34,** 310 (1987).
28. J. A. Cooper Jr. and D. F. Nelson, *J. appl. Phys.* **54,** 1445 (1983).
29. K.-Y. Ton, P.-K. Ko and R. G. Meyer, *IEEE J. Solid-St. Circuits* **SC-23,** 950 (1988).
30. P. Rossel, H. Martinot and G. Vassilieff, *Solid-St. Electron.* **19,** 51 (1976).
31. A. Modelli and S. Manzini, *Solid-St. Electron.* **31,** 99 (1988).
32. C. G. Sodini, T. W. Ekstedt and J. L. Moll, *Solid-St. Electron.* **25,** 833 (1982).
33. D. Frohman-Benchkowsky, *Proc. IEEE* **56,** 217 (1968).
34. J. P. Leburton, H. Gesch and G. Dorda, *Solid-St. Electron.* **24,** 763 (1981).
35. J. Rebollo, E. Figueras, J. Millán, E. Lora-Tamayo and F. Serra-Mestres, *Solid-St. Electron.* **30,** 177 (1987).
36. V. V. Bachurin, V. P. D'yakonov and T. A. Samoilova, *Izvestiya VUZ. Radioelektronika* **26,** 41 (1983).
37. P. Ratnam and C. A. T. Salama, *IEEE Trans. Electron Devices* **ED-31,** 1289 (1984).
38. M. H. White, F. Vandewiele and J. P. Lambot, *IEEE Trans. Electron Devices* **ED-27,** 899 (1980).
39. D. Roychoudhury and P. K. Basu, *Solid-St. Electron.* **19,** 656 (1976).

APPENDIX A

A Qualitative Analysis of the Q_i Models

Let us assume $U_{GSeff} \geqslant 0$. It is evident: D, $2\varphi_B$, $U_T > 0$. From eqn (14) follows $\partial V/\partial y > 0$, namely V increases monotonically along the channel (from the source towards the drain). For the starting Q_i model (2)(4) the next theorem follow:

(1) φ_S decreases monotonically, while the surface potential $V + \varphi_S - U_{BS}$ increases monotonically along the channel. Proof: $\partial\varphi_S/\partial y = \partial\varphi_S/\partial V \cdot \partial V/\partial y$. Differentiation

eqn (2) yields $\partial\varphi_S/\partial V < 0$. For the surface potential follows: $\partial(V + \varphi_S)/\partial y = (1 + \partial\varphi_S/\partial V) \cdot \partial V/\partial y$. It is easy to see that $1 + \partial\varphi_S/\partial V > 0$. Consequence: Q_i decreases monotonically along the channel (because $V + \varphi_S$ increases monotonically). Therefore Q_i is minimal at the drain channel end. Consequently, at first the fail of the G.C.A. (entering into the saturation) occurs at $y = L_{eff}$.

(2) For the charge model (2)(4) a finite classical saturation voltage U_{DSsc} does not exist (U_{DSsc} is defined by $Q_i(U_{DSsc}) = 0$). Proof: The theorem follows directly from (2)(4). Namely: $U_{DSsc} \to \infty$, $Q_i(L_{eff}) \to 0$ ($\varphi_S \to -\infty$).

From (1), (2) follows that $Q_i(V) > 0$ holds for all U_{DS}: $0 \leqslant V \leqslant U_{DS}$.

In the analytical current model the charge Q_i is given with (4), where φ_S is determined with eqn (20). The substitution $\varphi_S(V)$ with φ_S^η changes qualitatively some behaviours of the Q_i model, as the next theorems show:

(3) Q_i decreases monotonically along the channel. Proof: Follows directly from (4), because V increases monotonically, while φ_S^η is constant. Consequence: Q_i becomes minimal at the drain channel end, where at first the fail of the G.C.A. occurs.

(4) By increasing U_{DS}: φ_S^η decreases for $\eta > 0$, φ_S^η is constant for $\eta = 0$, while $\varphi_S^\eta + U_{DS}$ increases. Proof: Differentiation (20) yields $\partial\varphi_S^\eta/\partial U_{DS}$. For $\eta > 0$ follows $\partial\varphi_S^\eta/\partial U_{DS} < 0$, while for $\eta = 0$ is $\partial\varphi_S^\eta = 0$ (independent of U_{DS}). Hence $1 + \partial\varphi_S^\eta/\partial U_{DS} > 0$ follows. Consequence: $Q_i(L_{eff})$ decreases by increasing U_{DS}.

(5) For $\eta < 1$ a finite U_{DSsc} exists, while for $\eta = 1$ it does not exist. Proof: For $\eta = 1$ follows evidently. For $\eta < 1$ the proof follows after the laborious, but simple analysis of the system (4)(20). Also $\eta \to 1$, $U_{DSsc} \to \infty$, $\varphi_S^\eta(U_{DSsc}) \to -\infty$ holds.

The consequence of (3), (4) and (5) is: If $\eta < 1$ then $Q_i(V) > 0$ holds for $0 \leqslant V \leqslant U_{DS} < U_{DSsc}$. If $\eta = 1$ then $Q_i(V) > 0$ holds for all $V \geqslant 0$. Hence, for practical calculations of the saturation voltage U_{DSs} an important consequence follows: In the case $\eta < 1$, at first we need to calculate U_{DSsc}. During an iterative procedure for the calculation of U_{DSs} a limitation $0 < U_{DSs} < U_{DSsc}$ ensures that the expressions in the current model are defined. There is not an upper limitation for $\eta = 1$: $0 < U_{DSs}$. The presented theorems are very important for proper and efficient computer implementations of the model.